HHS Public Access

Author manuscript

Analyst. Author manuscript; available in PMC 2015 October 28.

Published in final edited form as:

Analyst. 2015 September 28; 140(20): 6980–6989. doi:10.1039/c5an00908a.

Investigating changes in the gas-phase conformation of Antithrombin III upon binding of Arixtra using traveling wave ion mobility spectrometry (TWIMS)

Yuejie Zhao[a], **Arunima Singh**[b], **Lingyun Li**[c], **Robert J. Linhardt**[c], **Yongmei Xu**[d], **Jian Liu**[d], **Robert J. Woods**[b], and **I. Jonathan Amster**[a]

I. Jonathan Amster: jamster@uga.edu

[a]University of Georgia, Department of Chemistry, 140 Cedar Street, Athens, GA 30602-2556, USA

[b]University of Georgia, Complex Carbohydrate Research Center, Athens, GA, USA

[c]Rensselaer Polytechnic Institute, Center for Biotechnology & Interdisciplinary Studies, Department of Chemistry & Chemical Biology, Troy, NY, USA

[d]University of North Carolina, Eshelman School of Pharmacy, Division of Chemical Biology & Medicinal Chemistry, Chapel Hill, NC, USA

Abstract

We validate the utility of ion mobility to measure protein conformational changes induced by the binding of glycosaminoglycan ligands, using the well characterized system of Antithrombin III (ATIII) and Arixtra, a pharmaceutical agent with heparin (Hp) activity. Heparin has been used as a therapeutic anticoagulant drug for several decades through its interaction with ATIII, a serine protease inhibitor that plays a central role in the blood coagulation cascade. This interaction induces conformational changes within ATIII that dramatically enhance the ATIII-mediated inhibition rate. Arixtra is the smallest synthetic Hp containing the specific pentasaccharide sequence required to bind with ATIII. Here we report the first travelling wave ion mobility mass spectrometry (TWIMS) investigation of the conformational changes in ATIII induced by its interaction with Arixtra. Native electrospray ionization mass spectrometry allowed the gentle transfer of the native topology of ATIII and ATIII–Arixtra complex. IM measurements of ATIII and ATIII–Arixtra complex showed a single structure, with well-defined collisional cross section (CCS) values. An average 3.6% increase in CCS of ATIII occurred as a result of its interaction with Arixtra, which agrees closely with the theoretical estimation of the change in CCS based on protein crystal structures. A comparison of the binding behavior of ATIII under both denaturing and non-denaturing conditions confirmed the significance of a folded tertiary structure of ATIII for its biological activity. A Hp oligosaccharide whose structure is similar to Arixtra but missing the 3-*O* sulfo group on the central glucosamine residue showed a dramatic decrease in binding affinity towards ATIII, but no change in the mobility behavior of the complex, consistent with prior studies that suggested that 3-*O* sulfation affects the equilibrium constant for binding to ATIII, but not the mode of interaction. In contrast, nonspecific binding by a Hp tetrasaccharide

Correspondence to: I. Jonathan Amster, jamster@uga.edu.

showed more complex mobility behavior, suggesting more promiscuous interactions with ATIII. The effect of collisional activation of ATIII and ATIII–Arixtra complex were also assessed, revealing that the binding of Arixtra provided ATIII with additional stability against unfolding. Overall, our results validate the capability of TWIMS to retain the significant features of the solution structure of a protein–carbohydrate complex so that it can be used to study protein conformational changes induced by the binding of glycosaminoglycan ligands.

Introduction

Heparin (Hp) and heparan sulfate (HS) are highly sulfated, linear polysaccharides, consisting of disaccharide repeat units of 1–4 linked hexuronic acid and *N*-acetyl-glucosamine, and are members of a class of carbohydrates known as glycosaminogly-cans (GAGs).[1] The sequence of Hp and HS features three types of domains: highly sulfated (NS) domains, less or non-sulfated *N*-acetylated (NA) domains and partially sulfated domains (NA/NS). Some of these domains are selectively recognized by over hundreds of secreted and membrane associated human proteins.[2–5] By regulating the location, stability and activity of these interacting proteins, Hp and HS play crucial role in many important physiological and pathological processes.[6]

The Hp/HS induced, allosteric activation of Antithrombin (ATIII) is the most studied and best understood example of a specific GAG–protein interaction. The anticoagulant property of Hp was discovered in 1916, and it has been used for prophylaxis and treatment of venous thrombosis, thrombophlebitis and embolism since 1940s.[2] Antithrombin III (ATIII), a 58.2 kDa *N*-glycosylated mono-chain protein in the serpin (serine protease inhibitor) family of proteins, serves as a principal regulator of blood coagulation serine and cysteine proteinases including factor IXa, factor Xa, and thrombin. The inhibitory activity of ATIII is repressed until it is activated by Hp/HS cofactor, either from therapeutic Hp or endothelial cells surface HS proteoglycans at the site of a vascular injury.[7] The native tertiary structure of ATIII is centered at a five-stranded β-sheet A, in which the N-terminal hinge of a reactive center loop (RCL) is initially buried with an orientation unfavorable to react with target proteinases.[8] Recent studies also found that the constraint of the RCL also intensifies the repulsive exosite interactions which counteracts the favorable interaction between proteinases and exosite determinants on strand 3 of sheet C surrounding the RCL.[9]

The activation of ATIII occurs *via* its interaction with Hp, and more specifically, with a unique pentasaccharide sequence with a rare 3-*O* sulfo group.[2] Upon binding of Hp/HS, a local conformational change at the Hp-binding site (the N-terminal region, the N-terminal end of helix A and all of helix D) is triggered. This further induces conformational changes on the proteinase binding site on ATIII.[10,11] As a result of the allosteric activating structure arrangement, the RCL is released and the equilibrium between favorable and repulsive exosite interactions shifts to the favorable side.[12] Therefore, the formation and stabilization of ATIII–proteinase complex are promoted. The inhibitory rate of ATIII can be accelerated up to 150–500-fold by the binding of the specific Hp pentasaccharide domain against factors Xa, IXa and VIIa, and this rate can be accelerated up to 2000–200 000-fold by full-length Hp.[13]

As shown in the case of the interaction between ATIII and Hp/HS, a protein–ligand or protein–protein interaction is often characterized by a three dimensional conformational change of the protein in response to a specific biological function. Conventional solid-phase method (X-ray crystallography) and solution-phase method (NMR spectroscopy) allow elucidation of structural details of protein and protein complex, and the structures of ATIII and ATIII–Arixtra complex have been characterized in this fashion. However, there are issues including difficult sample preparation, lengthy data analysis and low sample compatibility, which reduce the widespread applicability of these methods to a wide variety of protein–GAG complexes.[14]

Ion mobility mass spectrometry (IMMS) is a rapid, sensitive and high-throughput gas-phase technique combing the advantages of both ESI mass spectrometry and ion mobility separation, and has gained much attention and recognition in the field of structural and dynamical biology.[15] IMMS separates gas-phase ions according to their mobility, an intrinsic property determined by size, shape and charge state of ions.[16] Travelling wave ion mobility spectrometry (TWIMS) is a commonly-used approach for IMMS, and is a commercially available product. In TWIMS, ion mobility separation takes place in an ion guide filled with a neutral gas. A radially confining potential barrier stops ion diffusion away from the path of the ion beam, while a continuous series of low voltage pulses called travelling waves push ions through the device.[17] Protein ions with larger collisional cross section (CCS) have lower mobility, undergo more frequent collisions and fall behind the traveling waves, with the result that they are transmitted more slowly than ions with higher mobility. The drift time of a protein ion can be related to its CCS and conformation though calibration with standards. The biological relevance of the measured CCS can be validated by comparison with theoretical CCSs generated from NMR or X-ray crystal structures.[18]

Due to the advantage of TWIMS to experimentally estimate the CCS of a gas phase ion in a rapid and sensitive manner, it has been applied by a number of researchers for studies of protein interactions: Leary and coworker have applied TWIMS to detect differences in the conformations of two classes of chemokines as well as the effect of degree of sulfation of Hp-like oligomers on Hp-chemokine interactions;[19] Ruotolo and coworkers have applied TWIMS to study the gas-phase conformational stability of wild-type tetrameric transthyretin and its disease-associated variants with and without ligand binding;[20] Robinson and coworkers have applied TWIMS to measure the quaternary structure of the trp RNA binding protein (TRAP) complex and how the addition of tryptophan or RNA enhances the stability of its ring topology;[21] Heck and coworkers have applied TWIMS to measure the CCSs of oligomeric viral capsid assembly of Hepatitis B virus (HBV) and norovirus;[22] Russell and coworkers have applied TWIMS to study how the binding of metal ions influences the conformation transition of human metallothionein-2A (MT) protein;[23] Bowers and coworkers have used IMMS to investigate the quaternary structure and self-assembling pathways of amyloid-β protein assemblies.[24] Though there are concerns regarding the extent to which the structure of a gas-phase ion matches the native structure of a protein in solution, numerous studies have established a good correspondence between the two, particularly for the short time periods of an IMMS measurement, and under carefully controlled experimental conditions.[25]

The ATIII–Hp interaction featured by its well-studied conformational change and high binding specificity represents an excellent model to test the applicability of the TWIMS approach to examine conformational changes associated with GAG–protein interactions. In this study, we applied the method of TWIMS to investigate the nature and extent of conformational change within ATIII induced by the binding of Arixtra, a synthetic analogue of the Hp pentasaccharide sequence known to bind this protein with high specificity.[26] TWIMS experiments were performed in order to answer these questions: Can the solution structure of ATIII survive the gas-phase environment in TWIMS and still maintain its activity to bind with Hp? Is TWIMS capable of detecting the small difference in CCS for ATIII that is induced by the binding of Arixtra? Do gas-phase ATIII ions exhibit selective binding with Arixtra compared to other structurally-similar compounds? Do the complexes of ATIII and Hp oligosaccharides lacking some of the features of the specific binding motif show similar or different behaviors in their ion mobility? Collectively, the answers to the following questions provide insight into the utility of an IM approach, and more specifically, a TWIMS approach, for studying conformational changes in proteins as a result of their GAG interactions.

Experimental

Reagents

All chemicals and solvents (ammonium acetate, methanol, water and formic acid) were of HPLC grade and purchased from Sigma-Aldrich. AT III was purchased from Aniara/Hyphen Biomed as lyophilized powder (West Chester, OH). Stock solution of ATIII was made by dissolving the lyophilized protein into HPLC-grade water and then stored at −80 °C. Arixtra was purchased from the hospital formulary and desalted on a BioGel P2 column BioRad (Hercules, CA, USA) before use. Modified Arixtra was chemoenzymatically synthesized as previously described.[27] The Hp tetrasaccharide was produced from naturally occurring source as previously described.[28] Protein calibrants (myoglobin from equine heart, cytochrome c from equine heart, avidin from egg white, concanavalin A from *Canavalia ensiformis* and bovine serum albumin) were purchased from Sigma-Aldrich as lyophilized powder.

Sample preparation

For MS analyses under denaturing conditions, ATIII was diluted in a water/methanol/formic acid solution (49.5 : 49.5 : 1, v/v/v) to a final concentration of 3 μM. For MS analyses under non-denaturing conditions, ATIII was diluted in 20 mM ammonium acetate buffer, pH 6.8, to a final concentration of 10 μM. ATIII–Hp complex was obtained by incubating ATIII with Arixtra or other Hp oligosaccharides at a molar ratio of 1 : 1 at room temperature. Protein calibrants were diluted in either denaturing solution or non-denaturing solution to a final concentration of 10 μM.

IMMS measurement

NanoESI-IMMS experiments were performed using a quadrupole-TWIM-TOF hybrid mass spectrometer (Synapt G2 HDMS, Waters Corp., Manchester, UK) in positive ionization mode. Protein samples were injected into the nanoESI source through a fused-silica emitter

(PicoTip New Objective, Woburn, MA) with a flow rate varying from 0.2–0.5 μl min^{-1}. Experimental parameters were carefully tuned to prevent the protein and protein complex from unfolding or losing integrity due to extensive activation while keeping substantial ion transmission. The applied experimental parameters were: capillary voltage, 1.5 kV; sampling cone voltage, 30 V; extraction cone voltage, 5 V; source temperature, 90 °C; flow rate of nitrogen in the IM ion guide, 50 ml min^{-1}; flow rate of helium in the helium cell, 180 mL min^{-1}; Trap collision energy, 0 V; transfer collision energy, 0 V. Different sets of wave height and corresponding wave velocity were used to optimize the mobility separation. The drift times of the calibrants and ATIII samples were measured when identical experimental conditions were stringently applied. Data analysis was performed with Mass-Lynx 4.1(Waters Corp., Manchester, UK).

CCS calibration

The biggest challenge of IMMS using TWIMS is proper calibration. Mobility is a unique property for a given ion, and depends only on the features of a protein ion and neutral gas (mass, charge, size and shape). The measured drift time of an ion is under the influence of many other factors, including experimental conditions (magnitude and velocity of travelling wave, pressure of neutral gas, temperature of the source and ion guide). Since the electric field in TWIMS is not uniform due to the existence of travelling wave voltages whose electric potential is changing over time and position within the IM ion guide, drift time acquired using TWIMS cannot be converted directly into a CCS. Instead, the CCS of an analyte needs to be determined based on an empirical relationship between the drift times of protein calibrants and their known CCSs obtained previously by conventional drift time IMS.[29]

Experimental CCSs were calibrated, as described in several published protocols.[18,29] Briefly, the CCSs of calibrants were corrected for their charge state and reduced mass with respect to the buffer gas. The drift times were corrected for mass-dependent flight time spent in the transfer ion guide and TOF mass analyzer and mass-independent flight time spent in the transfer ion guide. The natural logarithm of corrected CCSs were plotted against the natural logarithm of corrected drift times and a mathematical formula ($\ln\Omega' = A\ln t'_D + B$) was derived. The calibration coefficient *A* was extracted to calculate the effective drift times $t''_D : t''_D = t'^{A}_D \times z/(\mu^{1/2})$.[18] A calibration curve was generated by plotting the literature CCSs as a function of t''_D. As suggested by Ruotolo *et al.*, the correlation coefficient R^2 of the calibration curve should be higher than 0.98.[18] The experimental CCS of the analyte ion was derived from this calibration curve based on the measured drift time.

Another intrinsic problem for this experiment is that the calibrant library uses CCSs which were measured in helium while the TWIMS measurement uses an IM ion guide filled with nitrogen. However, the absolute error of CCS calibration derived from measuring CCS in different gases can be minimized when appropriate separation parameters are applied and when protein calibrants used to construct calibration curves are carefully selected.[30,31]

We have noted that CCS estimation was substantially improved by using native protein calibrants in the calibration, compared with using only denatured myoglobin (data not shown). Previous studies showed that CCS calibrated using only denatured calibrants were strongly influenced by separation conditions in TWIMS experiment. Therefore, including native calibrants of similar shape and nature as the analytes in the calibrant set greatly increased the accuracy of calibrated CCS of native ATIII and ATIII–Hp complex.[32]

A selected set of native and denatured protein calibrants, with a mass range from 12 kDa to 102 kDa and a CCS range from 2303 $Å^2$ to 5550 $Å^2$ were employed. The charge states and literature CCSs of these protein calibrants used to construct the calibration curve are listed in Table 1, selected from the Collision Cross Section Database, Bush Lab.[33] The mass range and CCS range chosen were broad enough to bracket the masses and drift times of ATIII and ATIII–Hp complex ions (Fig. 1), so no extrapolation of the calibration curve is necessary.

The separation parameters controlling the ion mobility separation were optimized, so that they fit both the analytes and calibrants. Multiple sets of separation parameters were applied to exclude the effect of electric field on the drift time measurement. The calibration curves constructed at wave height of 13, 15 and 17 V are shown in Fig. 1. R^2 values of 0.9919, 0.9944 and 0.9966 were observed for each trend line.

Theoretical calculation of CCSs

The missing residues in the PDB files for the ATIII–Arixtra complex (PDBid: 1E03) and ATIII (PDBid: 1E05)[34] were added using MODELLER.[35] In the complex, the protein was missing 5 residues from the N-terminus and 8 residues from a disordered portion of the N-terminus. The free protein lacked 2 residues from the N terminus and 12 residues from the disordered region that was missing in the protein in complex with Arixtra. Both forms also lacked one residue at the C-terminus.

Topology and coordinate files for the ATIII–Arixtra complex and free ATIII were generated using the tLeap program, employing the Protein ff99SB[36] and GLYCAM06 (version j)[37] parameters for the protein and GAGs, respectively. The net charge on each system was neutralized with the addition of appropriate number of Na^+ ion. The systems were solvated with TIP3P water model[38] in an octahedron box extending to at least 12 Å from any atom of the solute.

All MD simulations were performed with the GPU implementation of pmemd, pmemd.cuda_SPDP[39] in Amber14.[40] Energy minimization of the solvent was performed in an NVT ensemble (1000 steps of steepest descent, 24 000 steps of conjugate gradient), followed by a full system energy minimization (1000 steps of steepest descent, 24 000 steps of conjugate gradient). The systems were heated from 5 K to 300 K over 60 ps in an NVT ensemble, with a weak positional restraint (10 kcal mol^{-1} $Å^{-2}$) on the atoms in the solute. A Berendsen-type thermostat[41] with a time coupling constant of 1 ps, was utilized for temperature regulation. Equilibration and production was performed at constant pressure (NPT ensemble; 1 atm), with a pressure relaxation time of 1 ps. After the heating step the restraints were removed from the solute atoms, and the entire system was allowed to

equilibrate at 300 K for 1 ns. All covalent bonds involving hydrogen atoms were constrained using the SHAKE[42] algorithm, allowing a simulation time step of 2 fs. Scaling factors for 1–4 interactions were set to the recommended values of 1.0 and 1.2 for the GAG[37] and protein,[36] respectively, and a non-bonded interaction cutoff of 8.0 Å was employed. Long-range electrostatics were computed with the particle mesh Ewald (PME) method. Data were collected for 20 ns for both the systems. Post processing of the MD simulations was performed using ptraj[43] module of Amber and graphical representations of the results were generated with VMD.[44]

Theoretical CCSs of ATIII and ATIII–Arixtra complex were calculated on 30 frames from the last 5 ns of the simulation using MOBCAL.[45] Both the projection approximation (PA),[45] and trajectory method (TM)[46] were employed for the calculations. Additionally, for the simulation of ATIII in complex with Arixtra, the CCS was also calculated after removal of the ligand, in order to estimate the contribution of protein conformational change to the overall change in the CCS.

Results and discussion

Native mass spectrometry of unbound and Arixtra-bound ATIII

ATIII was first analyzed under non-denaturing condition without the addition of any Hp (Fig. 2a). The protein was represented by a single charge state envelope, indicating that only protein monomers existed under this experimental condition. Five charge states were observed from +17 to +13 over a range of *m*/*z* 3300–4700. Since the charge states detected by using native MS depend opon the three dimensional conformation of the protein ion, a narrow distribution of lower charge states indicates a folded and compact conformation with fewer basic sites exposed for protonation.[47] The three charge states, +16 to +14, were selected for further investigation since they were the most dominant charge states with relatively higher S/N. An average molecular weight of 57 876 ± 6 Da was obtained, in agreement with the literature molecular weight of ATIII (57 875 Da).[48]

ATIII was next incubated with a small molar excess of Arixtra. Two incubating times were examined to monitor the progress of the binding reaction: 1 h (Fig. 2b) and 12 h (Fig. 2c). The binding of Arixtra by ATIII did not change the charge state distribution observed for the native protein. An additional peak was observed for each charge state, corresponding to the formation of Arixtra–ATIII complex. An average mass increase of 1512 Da was measured for the new peaks, in good correspondence to the molecular weight of a single Arixtra molecule (1505 Da). To confirm the binding stoichiometry, titration experiments with different molar ratios were examined, but increasing the amount of Arixtra did not result in the formation of any new peaks. After 12 h of incubation, only the peaks corresponding to Arixtra bound to ATIII in a 1 : 1 ratio were present (Fig. 2c). Since longer incubation time allowed the binding reaction to go to completion, this result indicates that the ATIII only presents one binding site for Arixtra, in accordance with the 1 : 1 binding stoichiometry between ATIII and Arixtra reported previously.[49] All of these observations suggest that the solution structure of ATIII survives the ionization process and the environment of the TWIMS instrument.

Interestingly, the intensity ratio between ATIII with and without Arixtra varied with charge state. The ratio for +17, +16, +15 and +14 were 0.69, 1.02, 3.07 and 5.75, respectively. It is evident that the intensity ratio increases with the decrease of charge state, suggesting weakening in the binding affinity with the increase of charge state. One possible explanation is that the lower charge states are more representative of the native structure of ATIII due to a lowering of charge–charge repulsion.

TWIMS of ATIII and its complex with Arixtra

To investigate whether the protein conformational change caused by the interaction between ATIII and Arixtra can be detected by TWIMS, ion mobility measurements were performed on the gas-phase ATIII and Arixtra-bound ATIII ions. The measured drift times of each charge state of ATIII and Arixtra-bound ATIII are shown in Fig. 3, at a wave height of 17 V. One narrow drift time distribution was observed for each charge state of ATIII, indicating the presence of a single compact and folded conformation for the ATIII ions. For Arixtra–ATIII complex, a single narrow peak at higher drift time was observed for each charge state, implying that binding of Arixtra causes a change in the folded conformation of ATIII, leading to a specific structure with a larger CCS. These observations suggest that the tertiary structures of ATIII and the non-covalent Arixtra–ATIII complex are stable in the TWIMS experiment.

After calibration, the measured drift times for ATIII and its complex with Arixtra have been converted to CCSs, shown in Table 2. For each charge state, the reported CCS was an average from triplicate experiments, and was found to have a 0.6% relative standard deviation. The binding of Arixtra induces a 3.6% increase in CCS of ATIII, several times larger than the standard deviation in the measurements. The conformational change was highly reproducible, and was observed for each charge state, as well as for a variety of wave heights and wave velocities. The drift times and peak shape measured for residual bound ATIII, which is present at moderate abundance in the mass spectrum of the 1 hour mixture, Fig. 2b, were the same as the drift times measurements for the ATIII peaks in the mass spectrum of the pure protein sample, Fig. 2a, evidence of the stability of the drift time measurements over different times and different samples.

Specificity and selectivity of ATIII–Arixtra interaction

To test the specificity of the interaction between ATIII and Hp, two control experiments were applied by altering the structure and conformation of both ATIII and its binding partner.

The first control experiment was to test the binding capability of ATIII after being denatured due to the presence of organic solvents under harsh pH condition (49.5 water : 49.5 methanol : 1 formic acid). Denatured ATIII was incubated with Arixtra at a molar ratio of 1 : 3 for 12 h and sprayed in a denaturing solution (Fig. 4). A wide distribution of higher charge states from +47 to +23 were observed, in contrast to the narrow distribution of lower charge states under non-denaturing conditions. No peaks corresponding to the formation of ATIII–Arixtra complex were observed for these higher charge states, indicating that the fully denatured ATIII loses its capability to bind with Arixtra. This control eliminates the

concern that the complex formed between ATIII and Arixtra is non-specific, and results from the columbic attraction of a positively charged protein with an anionic carbohydrate. A mass scale expansion of the higher mass range of the denatured ATIII shows Arixtra-bound ATIII peaks for charge states lower than +20 (Fig. 4, inset). It is possible that these relatively low charge states may represent some partially folded structures of ATIII.

A broad drift time distribution with multiple features was observed for each charge state of denatured ATIII (data not shown) while a single sharp peak was observed for native ATIII. This observation indicates that the fully extended or partially unfolded structures of ATIII have higher flexibility than the folded structures, and adopt multiple conformations in the gas phase.

Previous studies have collected evidence that Hp binding sites on proteins are more than clustered basic amino acid residues. Instead, several structural elements (loops, α-helices and β-strands) have been found in Hp binding sites, implying that specific spacing and spatial patterns of the Hp-binding basic residues are essential in Hp-protein interactions.[3,5,50] As in the case of ATIII–Hp binding, the folded, compact conformation of ATIII allows a spatial alignment of the Hp-binding basic residues which were widely distributed in the sequence.[11,51] This alignment facilitates the formation of a basic patch over several helices and the N-terminal region of ATIII, which provides a binding site for Hp. In this control experiment, denaturing the protein led to a substantial alternation of the topology of the Hp binding sites,[4] therefore disrupting the high affinity binding interaction between ATIII and Hp. Our observation revealed the importance of a folded, compact structure of ATIII to maintain its biological activity.

A second control experiment was performed to test the binding specificity between ATIII and Arixtra induced by the pattern of sulfation. Arixtra has eight sites of sulfation, with a sequence of: $GlcNSO_3$, $6SO_3$-GlcA-$GlcNSO_3$, $3SO_3$, $6SO_3$-IdoA2SO_3-$GlcNSO_3$, $6SO_3$, as shown in Fig. 5. The ATIII binding behavior of a Hp hexasaccharide and a Hp tetrasaccharide, with the structures shown in Fig. 5, were examined. The sulfation pattern of the Hp hexasaccharide closely resembles that of Arixtra, minus the 3-*O* sulfo group on the central glucosamine. The Hp tetrasaccharide lacks two sulfate groups and a monosaccharide on the non-reducing end, compared to the structure of Arixtra.

After incubating ATIII and the hexasaccharide, peaks corresponding to the hexasaccharide-bound ATIII complex, Fig. 2d, were observed, but in much lower abundance compared to Arixtra, for the same incubation time and Hp concentration. Increasing the Hp concentration produced only a small increase in the intensity of the hexasaccharide-bound ATIII complex peaks. This reaction never went to completion, as can be inferred from the presence of unbound ATIII ions which dominated the mass spectra, even after longer incubation time. All of these observations indicate that the binding affinity of the hexasaccharide towards ATIII is much lower than Arixtra, consistent with previous studies.[52] Similar results were observed for the binding between ATIII and the tetrasaccharide, with the peaks corresponding to ATIII–tetrasaccharide complex in even lower abundance (results not shown). Our results suggest that the hexasaccharide and tetrasaccharide both have reduced

binding affinities for ATIII. The data confirms the significant contribution of the rare 3-*O* sulfation in Hp-protein interaction.

The drift time distributions of ATIII-negative control complexes were measured and only the results for +15 charge state are shown in Fig. 6. For the complex of ATIII and hexasaccharide, a narrow drift time distribution was observed (Fig. 6b), almost identical to that measured for ATIII–Arixtra complex (Fig. 6c). The drift time measured for hexasaccharide-bound ATIII was the same as that measured for Arixtra-bound ATIII, which agrees with a previous study that concluded that removing the 3-*O* sulfo group affected the equilibrium of native ATIII and activated ATIII but not the conformational change associated with the equilibrium.[53] In other words, this control Hp oligosaccharide retains the specificity of binding, but has a reduced binding affinity.

In strong contrast, the Hp tetrasaccharide-ATIII complex revealed a very different behavior, exhibiting a broad peak with many features in the drift time spectrum, Fig. 6a, suggesting several structures for the complex. We interpret these as reduced specificity in the binding of the Hp ligand. The drift times measured for Hp tetrasaccharide-bound ATIII were smaller than that measured for Arixtra-bound ATIII, suggesting that the binding of the Hp tetrasaccharide may induce less of a conformational change within ATIII, due to the loss of several essential components from the specific pentasaccharide sequence.[54]

The results of these control experiments are consistent with the known high-affinity, specific interaction between ATIII and Hp. It requires more than the existence of negatively charged functional groups on the Hp and positively charged residues on the protein. Instead, a well-defined three-dimensional presentation of the negatively charged groups in the Hp and a well-defined tertiary structure of the protein are critical to the specificity of ATIII–Arixtra binding.

Gas phase stability of ATIII and ATIII in complex with Arixtra

Previous studies have shown that the addition of a ligand or counter ions brings in additional conformational stability of protein ions against collisional activation.[55,56] To test whether the specific binding of Arixtra has altered the conformational stability of ATIII, we performed a series of experiments with incremental changes in trapping collisional energy (CE) from 5 V to 30 V being applied to ATIII with and without Arixtra in the trap ion guide prior to ion mobility separation. This probes the susceptibility to collision-induced unfolding for native ATIII and the ATIII–Arixtra complex.

The resulting drift time distributions of +15 charge state of both ATIII and ATIII–Arixtra complex are shown in Fig. 7. Each drift time distribution was fitted with a minimum number of Gaussian distributions according to its shape using the peak analyzer in OriginPro 8.5.0 software (OriginLab Corporation, MA), as described previously.[57] Each Gaussian distribution generated as part of the fitness represents a potentially stabilized gas-phase conformation.

At a trapping CE of less than 20 V (data not shown) or equal to 20 V, a single, narrow peak was observed for both ATIII and ATIII–Arixtra complex, suggesting a single conformation

of the protein and its Hp-bound complex. The behavior of ATIII and ATIII–Arixtra complex started to deviate at elevated activation energy. For ATIII, a shoulder appeared on the high-drift-time side of the original peak when the trapping CE was raised to 22.5 V. Four Gaussian distributions fit this drift time distribution, indicating that several partially unfolded or unfolded conformations of gas-phase ATIII ions were present at this collision energy. At a CE of 25 V, the abundance of the shoulder peak clearly increased. Two distinct populations of higher mobility (from 10.37 to 14.10 ms) and lower mobility (from 14.24 to 18.11 ms) conformations were observed, each modeled by two or three Gaussian distributions. At a CE of 27.5 V, a broad drift time distribution resolved by eight Gaussian distributions was observed, indicating the presence of a series of protein conformations with different degrees of unfolding.

In contrast, for a range of trapping CE from 0 to 25 V, the drift time distributions of ATIII–Arixtra complex remained unaffected, evidenced by a single, narrow peak in the drift time spectrum. A lower mobility peak corresponding to partially unfolded conformation of ATIII complex was not formed until a trapping CE as high as 27.5 V was applied, while the higher mobility peak corresponding to the folded structure was still the dominant peak. Clearly, ATIII, when complexed with Arixtra, is more stable than ATIII itself, also consistent with solution-phase behavior of this system.[58]

Previous studies showed that the binding of Hp/HS improves conformational stability of some proteins against heat and proteolysis.[59] The additional stability is also related to the activity of proteins.[58] Our results showed that ATIII–Arixtra complex possesses higher conformational stability than ATIII itself, indicating that the stability of Hp-activated ATIII may be a driving factor for its biological activity, which is responsible for shifting the conformational equilibrium towards greater stability.

Comparison of experimental CCS with theoretical CCS

Theoretical CCSs estimated from X-ray crystal structures of ATIII and Arixtra-bound ATIII were compared with experimentally measured CCSs. The PDB files of ATIII and ATIII–Arixtra complex display two ATIII molecules, one in the inhibitory form and the other in the latent form.[34] Only the inhibitory structure was used for the CCS calculation. In addition, N-linked oligosaccharide chains are present in the structures in both PDF files. We chose to leave the oligosaccharides out of the CCS calculation. The N-linked oligosaccharides are not thought to participate in Hp binding, so they are expected to contribute equally to the CCS of ATIII and ATIII–Arixtra complex. As we are interested in the conformation change within the protein rather than the absolute measurement of CCSs, the glycosylation-free estimation of CCS should allow us a direct and simple observation of the conformational change. We added the missing H-atoms to the crystal structures since their effect may not be ignored in the accurate estimation of the subtle conformational change.

The calculated CCSs of native ATIII were 3010.1 $Å^2$ estimated using PA and 3900.5 $Å^2$ estimated using TM. The calculated CCSs of Arixtra-bound ATIII were 3120.2 $Å^2$ estimated using PA and 4033.3 $Å^2$ estimated using TM (Table 3). The experimental CCSs for the lowest charge state of native ATIII and ATIII–Arixtra complex were 3467.9 $Å^2$ and 3607.1 $Å^2$, respectively, comparable with those theoretical measurements.

The experimental CCS is approximately 12.1% less than the theoretical CCSs estimated using TM and 15.4% higher than that estimated using PA. These observations are consistent with previous studies on other proteins, which found that reasonable experimental CCSs should lie in between the theoretical estimates made using PA and TM. The experimental CCSs should be smaller than TM results, due to the collapsed structure of protein ions in the gas-phase in response to desolvation.[14,60,61] Ignoring the long-range interaction with the neutral gas, collision effect and scattering process, PA results are on average 15% smaller than the experimental CCSs,[62] in agreement with our observation.

It is noteworthy that there is close agreement between the relative changes in the CCS measured experimentally *versus* those determined by theoretical calculations. The averaged experimental conformational change was 3.6%, while the calculated conformational change was 3.7% for PA results and 3.4% for TM results, respectively. The contribution of the protein conformational change to the overall increase in the CCS was calculated to be 47.8% using the PA method, and 52.5% using the TM method. It would be safe to say that about 50% of the increase in CCS for Arixtra bound ATIII comes from the protein, while the remaining increase is due to the presence of Arixtra itself. These results show that the TWIMS experiment generates gas-phase ATIII and Arixtra-bound ATIII ions with conformations that match the solution structure closely, thus allowing and accurate measurement of the conformational changes in ATIII upon Arixtra binding.

Conclusions

TWIMS was found to provide data that is consistent with the known details of ATIII–Arixtra binding. Our mass spectra showed the formation of a 1 : 1 complex of ATIII with Arixtra, and the corresponding IM spectra were consistent with a single, folded gas-phase conformation of ATIII in its free and Arixtra-bound form, evidenced by a single narrow drift time distribution in both cases. CCSs derived from these data showed that the binding of Arixtra to ATIII caused a 3.6% increase of ATIII's CCS. Both the absolute CCSs of ATIII and Arixtra-bound ATIII ions as well as the degree of CCS change were in agreement with theoretical CCSs calculated using coordinates from their X-ray crystal structures.

Furthermore, the selectivity and specificity of Hp-ATIII binding known from solution measurements appeared to survive the translation of the ions into the gas-phase, as revealed by the control experiments. Disrupting the folded structure of ATIII caused the loss of its binding affinity towards Arixtra. Removing the 3-*O* sulfo group from the known Hp binding sequence resulted in substantial reduction of the abundance of ATIII–Hp complex but did not change the drift time behavior, as expected based on known solution behavior. These two control experiments not only confirmed the biological relevance of the native ATIII and Arixtra-bound ATIII ions that we observed, but also provided evidence to support the existence and significance of the specificity of the ATIII–Hp interaction. A control experiment using a Hp tetrasaccharide with a different pattern of sulfation than the known consensus sequence not only showed a substantially reduced affinity for ATIII, but also showed a reduction in specificity of binding, evidenced by a broad drift time distribution, consistent with a variety of structures for the complex. Moreover, the TWIMS measurement

showed the stabilizing effect of Arixtra binding on the ATIII folded structure. This result also matched solution studies of ATIII and its Hp complexes.

Collectively, these results highlight the advantages of TWIMS for investigating GAG–protein interactions at the molecular level. Future applications of this approach will be useful for gaining a better understanding of the biological processes mediated by other GAG–protein interactions.

Acknowledgments

YZ, AS, RJW and IJA acknowledge generous financial support from the National Institutes of Health, grant P41 GM103390. LL, RJL, YZ, and IJA acknowledge generous financial support from the National Institutes of Health, grant R01 GM38060. YX and JL acknowledge generous financial support from the National Institutes of Health, grants R01 HL094463 and U01 GM102137.

References

1. Rabenstein DL. Nat Prod Rep. 2002; 19:312–331. [PubMed: 12137280]
2. Gandhi NS, Mancera RL. Chem Biol Drug Des. 2008; 72:455–482. [PubMed: 19090915]
3. Hileman RE, Fromm JR, Weiler JM, Linhardt RJ. Bioessays. 1998; 20:156–167. [PubMed: 9631661]
4. Raman R, Sasisekharan V, Sasisekharan R. Chem Biol. 2005; 12:267–277. [PubMed: 15797210]
5. Xu D, Esko JD. Annu Rev Biochem. 2014; 83:129–157. [PubMed: 24606135]
6. Capila I, Linhardt RJ. Angew Chem, Int Ed. 2002; 41:390–412.
7. Koide, T. Recent Advances in Thrombosis and Hemostasis 2008. Springer; 2008. p. 177-189.
8. Langdown J, Belzar KJ, Savory WJ, Baglin TP, Huntington JA. J Mol Biol. 2009; 386:1278–1289. [PubMed: 19452598]
9. Gettins PG, Olson ST. J Biol Chem. 2009; 284:20441–20445. [PubMed: 19401470]
10. Whisstock JC, Pike RN, Jin L, Skinner R, Pei XY, Carrell RW, Lesk AM. J Mol Biol. 2000; 301:1287–1305. [PubMed: 10966821]
11. Jin L, Abrahams JP, Skinner R, Petitou M, Pike RN, Carrell RW. Proc Natl Acad Sci U S A. 1997; 94:14683–14688. [PubMed: 9405673]
12. Olson ST, Richard B, Izaguirre G, Schedin-Weiss S, Gettins PG. Biochimie. 2010; 92:1587–1596. [PubMed: 20685328]
13. Olson ST, Swanson R, Raub-Segall E, Bedsted T, Sadri M, Petitou M, Hérault JP, Herbert JM, Björk I. Thromb Haemostasis. 2004; 92:929–939. [PubMed: 15543318]
14. Lanucara F, Holman SW, Gray CJ, Eyers CE. Nat Chem. 2014; 6:281–294. [PubMed: 24651194]
15. Uetrecht C, Rose RJ, van Duijn E, Lorenzen K, Heck AJ. Chem Soc Rev. 2010; 39:1633–1655. [PubMed: 20419213]
16. Kanu AB, Dwivedi P, Tam M, Matz L, Hill HH. J Mass Spectrom. 2008; 43:1–22. [PubMed: 18200615]
17. Giles K, Pringle SD, Worthington KR, Little D, Wildgoose JL, Bateman RH. Rapid Commun Mass Spectrom. 2004; 18:2401–2414. [PubMed: 15386629]
18. Ruotolo BT, Benesch JL, Sandercock AM, Hyung SJ, Robinson CV. Nat Protocols. 2008; 3:1139–1152. [PubMed: 18600219]
19. Seo Y, Andaya A, Bleiholder C, Leary JA. J Am Chem Soc. 2013; 135:4325–4332. [PubMed: 23418647]
20. Hyung S-J, Robinson CV, Ruotolo BT. Chem Biol. 2009; 16:382–390. [PubMed: 19389624]
21. Ruotolo BT, Giles K, Campuzano I, Sandercock AM, Bateman RH, Robinson CV. Science. 2005; 310:1658–1661. [PubMed: 16293722]
22. Uetrecht C, Barbu IM, Shoemaker GK, van Duijn E, Heck AJ. Nat Chem. 2011; 3:126–132. [PubMed: 21258385]

23. Chen SH, Chen L, Russell DH. J Am Chem Soc. 2014; 136:9499–9508. [PubMed: 24918957]
24. Bernstein SL, Dupuis NF, Lazo ND, Wyttenbach T, Condron MM, Bitan G, Teplow DB, Shea JE, Ruotolo BT, Robinson CV, Bowers MT. Nat Chem. 2009; 1:326–331. [PubMed: 20703363]
25. Williams DM, Pukala TL. Mass Spectrom Rev. 2013; 32:169–187. [PubMed: 23345084]
26. Petitou M, van Boeckel CA. Angew Chem, Int Ed. 2004; 43:3118–3133.
27. Xu Y, Cai C, Chandarajoti K, Hsieh PH, Li L, Pham TQ, Sparkenbaugh EM, Sheng J, Key NS, Pawlinski R, Harris EN, Linhardt RJ, Liu J. Nat Chem Biol. 2014; 10:248–250. [PubMed: 24561662]
28. Xiao Z, Zhao W, Yang B, Zhang Z, Guan H, Linhardt RJ. Glycobiology. 2011; 21:13–22. [PubMed: 20729345]
29. Smith DP, Knapman TW, Campuzano I, Malham RW, Berryman JT, Radforda SE, Ashcrofta AE. Cell. 2009; 12:13. [eqn (1)].
30. Salbo R, Bush MF, Naver H, Campuzano I, Robinson CV, Pettersson I, Jørgensen TJ, Haselmann KF. Rapid Commun Mass Spectrom. 2012; 26:1181–1193. [PubMed: 22499193]
31. Jurneczko E, Kalapothakis J, Campuzano ID, Morris M, Barran PE. Anal Chem. 2012; 84:8524–8531. [PubMed: 22974196]
32. Bush MF, Hall Z, Giles K, Hoyes J, Robinson CV, Ruotolo BT. Anal Chem. 2010; 82:9557–9565. [PubMed: 20979392]
33. http://depts.washington.edu/bushlab/ccsdatabase.
34. McCoy AJ, Pei XY, Skinner R, Abrahams JP, Carrell RW. J Mol Biol. 2003; 326:823–833. [PubMed: 12581643]
35. Šali A, Blundell TL. J Mol Biol. 1993; 234:779–815. [PubMed: 8254673]
36. Hornak V, Abel R, Okur A, Strockbine B, Roitberg A, Simmerling C. Proteins: Struct, Funct, Bioinf. 2006; 65:712–725.
37. Kirschner KN, Yongye AB, Tschampel SM, González-Outeiriño J, Daniels CR, Foley BL, Woods RJ. J Comput Chem. 2008; 29:622–655. [PubMed: 17849372]
38. Jorgensen WL, Chandrasekhar J, Madura JD, Impey RW, Klein ML. J Chem Phys. 1983; 79:926–935.
39. Götz AW, Williamson MJ, Xu D, Poole D, Le Grand S, Walker RC. J Chem Theory Comput. 2012; 8:1542–1555. [PubMed: 22582031]
40. Case, DA.; Berryman, JT.; Betz, RM.; Cerutti, DS.; Cheatham, TE., III; Darden, TA.; Duke, RE.; Giese, TJ.; Gohlke, H.; Goetz, AW.; Homeyer, N.; Izadi, S.; Janowski, P.; Kaus, J.; Kovalenko, A.; Lee, TS.; LeGrand, S.; Li, P.; Luchko, T.; Luo, R.; Madej, B.; Merz, KM.; Monard, G.; Needham, P.; Nguyen, H.; Nguyen, HT.; Omelyan, I.; Onufriev, A.; Roe, DR.; Roitberg, A.; Salomon-Ferrer, R.; Simmerling, CL.; Smith, W.; Swails, J.; Walker, RC.; Wang, J.; Wolf, RM.; Wu, X.; York, DM.; Kollman, PA. AMBER 2015. University of California; San Francisco: 2015.
41. Berendsen HJ, Postma JPM, van Gunsteren WF, DiNola A, Haak J. J Chem Phys. 1984; 81:3684–3690.
42. Ryckaert JP, Ciccotti G, Berendsen HJ. J Comput Phys. 1977; 23:327–341.
43. Roe DR, Cheatham TE III. J Chem Theory Comput. 2013; 9:3084–3095.
44. Humphrey W, Dalke A, Schulten K. J Mol Graphics. 1996; 14:33–38.
45. Mesleh M, Hunter J, Shvartsburg A, Schatz G, Jarrold M. J Phys Chem. 1996; 100:16082–16086.
46. Shvartsburg AA, Schatz GC, Jarrold MF. J Chem Phys. 1998; 108:2416–2423.
47. Chowdhury SK, Katta V, Chait BT. J Am Chem Soc. 1990; 112:9012–9013.
48. Fermas S, Gonnet F, Varenne A, Gareil P, Daniel R. Anal Chem. 2007; 79:4987–4993. [PubMed: 17536781]
49. Abzalimov RR, Dubin PL, Kaltashov IA. Anal Chem. 2007; 79:6055–6063. [PubMed: 17658885]
50. Lindahl U, Li Jp. Int Rev Cell Mol Biol. 2009; 276:105–159. [PubMed: 19584012]
51. Huntington JA, Olson ST, Fan B, Gettins PG. Biochemistry. 1996; 35:8495–8503. [PubMed: 8679610]
52. Johnson DJ, Huntington JA. Biochemistry. 2003; 42:8712–8719. [PubMed: 12873131]
53. Richard B, Swanson R, Olson ST. J Biol Chem. 2009; 284:27054–27064. [PubMed: 19661062]

54. Desai UR, Petitou M, Björk I, Olson ST. J Biol Chem. 1998; 273:7478–7487. [PubMed: 9516447]
55. Hopper JT, Oldham NJ. J Am Soc Mass Spectrom. 2009; 20:1851–1858. [PubMed: 19643633]
56. Han L, Hyung SJ, Mayers JJ, Ruotolo BT. J Am Chem Soc. 2011; 133:11358–11367. [PubMed: 21675748]
57. Shi H, Pierson NA, Valentine SJ, Clemmer DE. J Phys Chem B. 2012; 116:3344–3352. [PubMed: 22315998]
58. Lima MA, Hughes AJ, Veraldi N, Rudd TR, Hussain R, Brito AS, Chavante SF, Tersariol II, Siligardi G, Nader HB. Med Chem Comm. 2013; 4:870–873.
59. Gallagher JT. J Clin Invest. 2001; 108:357. [PubMed: 11489926]
60. Jurneczko E, Barran PE. Analyst. 2011; 136:20–28. [PubMed: 20820495]
61. Scarff CA, Thalassinos K, Hilton GR, Scrivens JH. Rapid Commun Mass Spectrom. 2008; 22:3297–3304. [PubMed: 18816489]
62. Hall Z, Politis A, Bush MF, Smith LJ, Robinson CV. J Am Chem Soc. 2012; 134:3429–3438. [PubMed: 22280183]

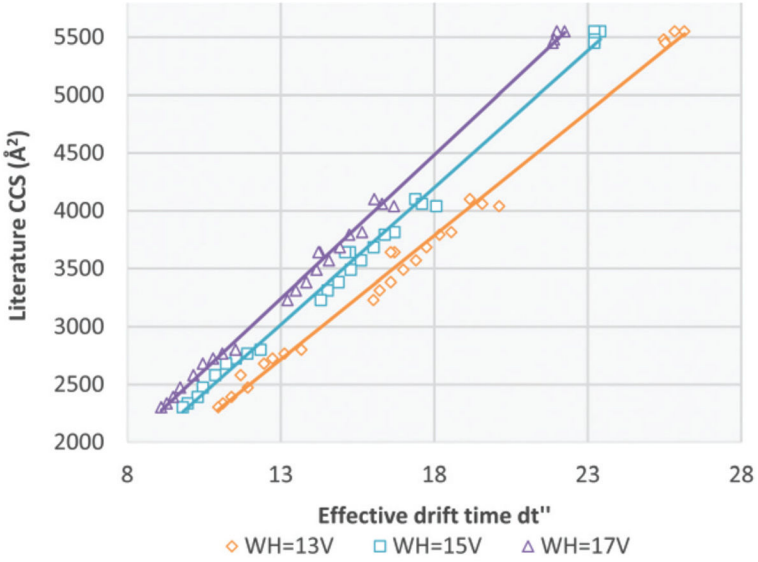

Fig. 1.

The calibration curves were constructed at three wave heights, combining data from cytochrome c, myoglobin, avidin, BSA and concanavalin A, displayed as literature CCS *vs.* effective drift time for each charge state.

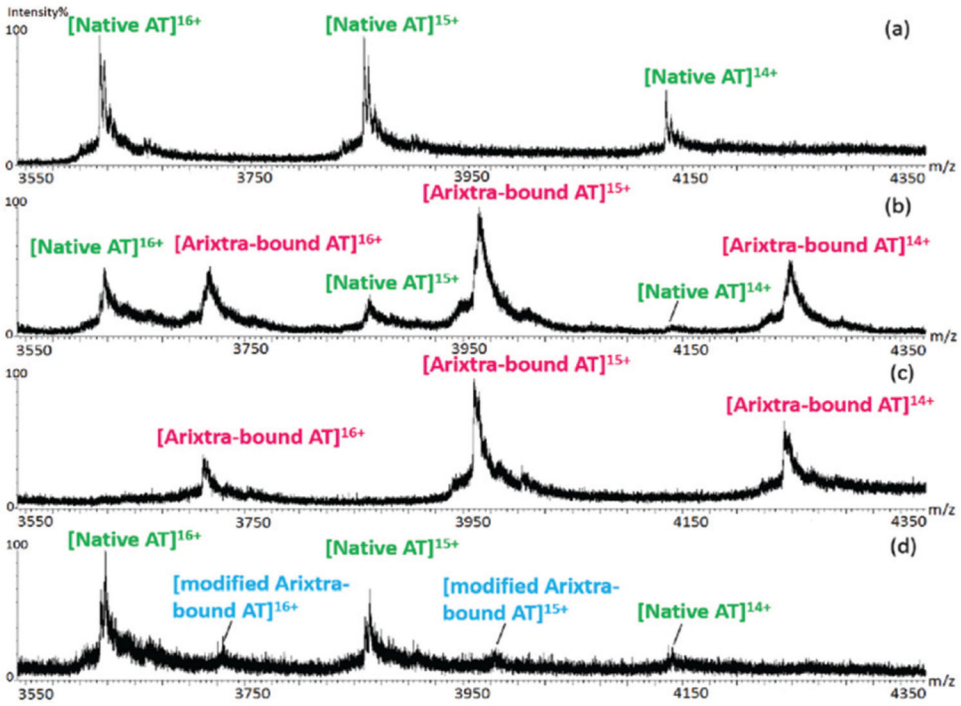

Fig. 2.

Electrospray ionization mass spectra, obtained under non-denaturing conditions, of (a) ATIII; (b) ATIII incubated with Arixtra for 1 h; (c) ATIII incubated with Arixtra for 12 h; (d) ATIII incubated with the Arixtra-like hexasaccharide, minus 3-*O*-sulfation, for 12 h.

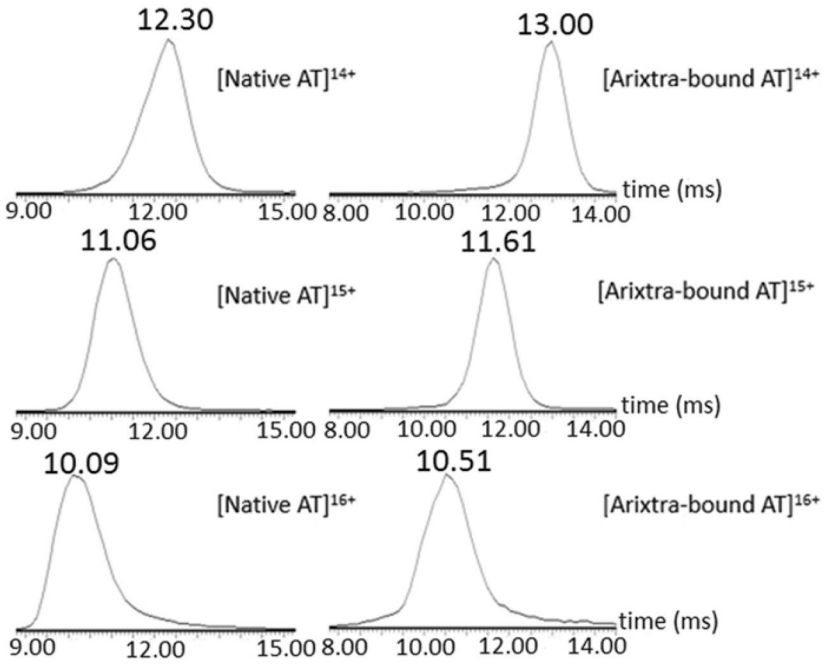

Fig. 3.

Drift timed distributions (ms) of the dominant charge states (+14–+16) of native ATIII and Arixtra-bound ATIII, at a wave height of 17 V.

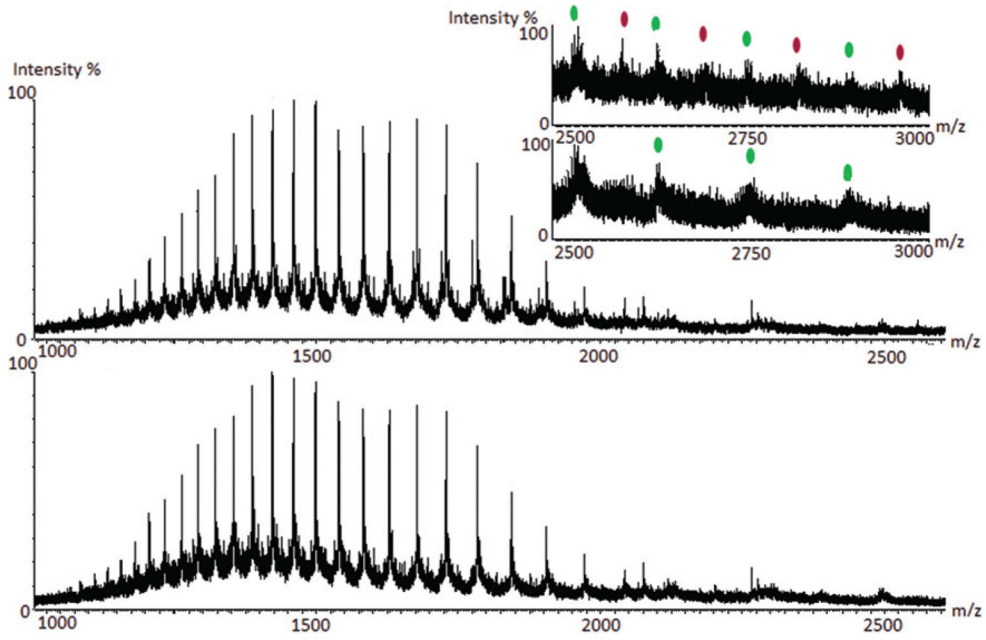

Fig. 4.

Electrospray ionization mass spectra of denatured ATIII with (upper) and without (lower) addition of Arixtra; The inset shows an expansion of the mass range (2500 *m*/*z*–3000 *m*/*z*) of the two spectra. Unbound ATIII peaks were labeled with green and Arixtra-bound peaks were labeled with purple.

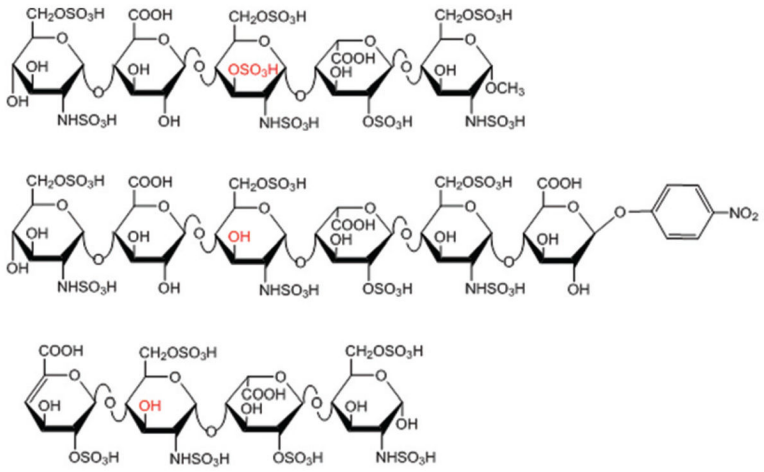

Fig. 5.

Structures of Arixtra (dp5 with 8 SO_3) (upper), modified Arixtra (dp6 with 7 SO_3) (middle) and the Hp tetrasaccharide (dp4 with 6 SO_3) (below).

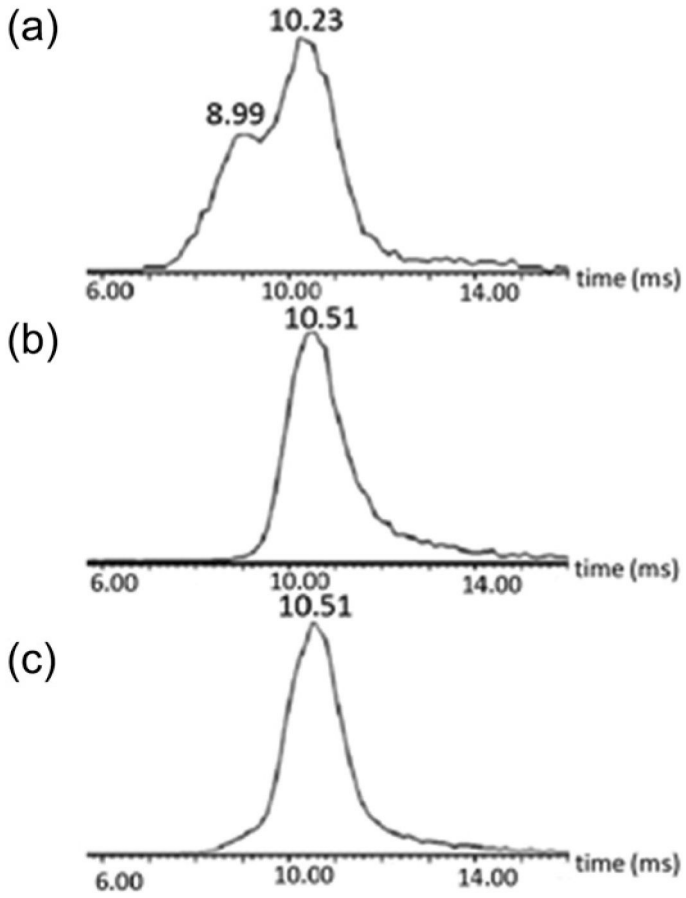

Fig. 6.

Drift time distributions (ms) of the +15 charge state of ATIII in complex with compounds, shown in Fig. 5, the Hp tetrasaccharide (a), modified Arixtra (b) and Arixtra (c), at a wave height of 17 V.

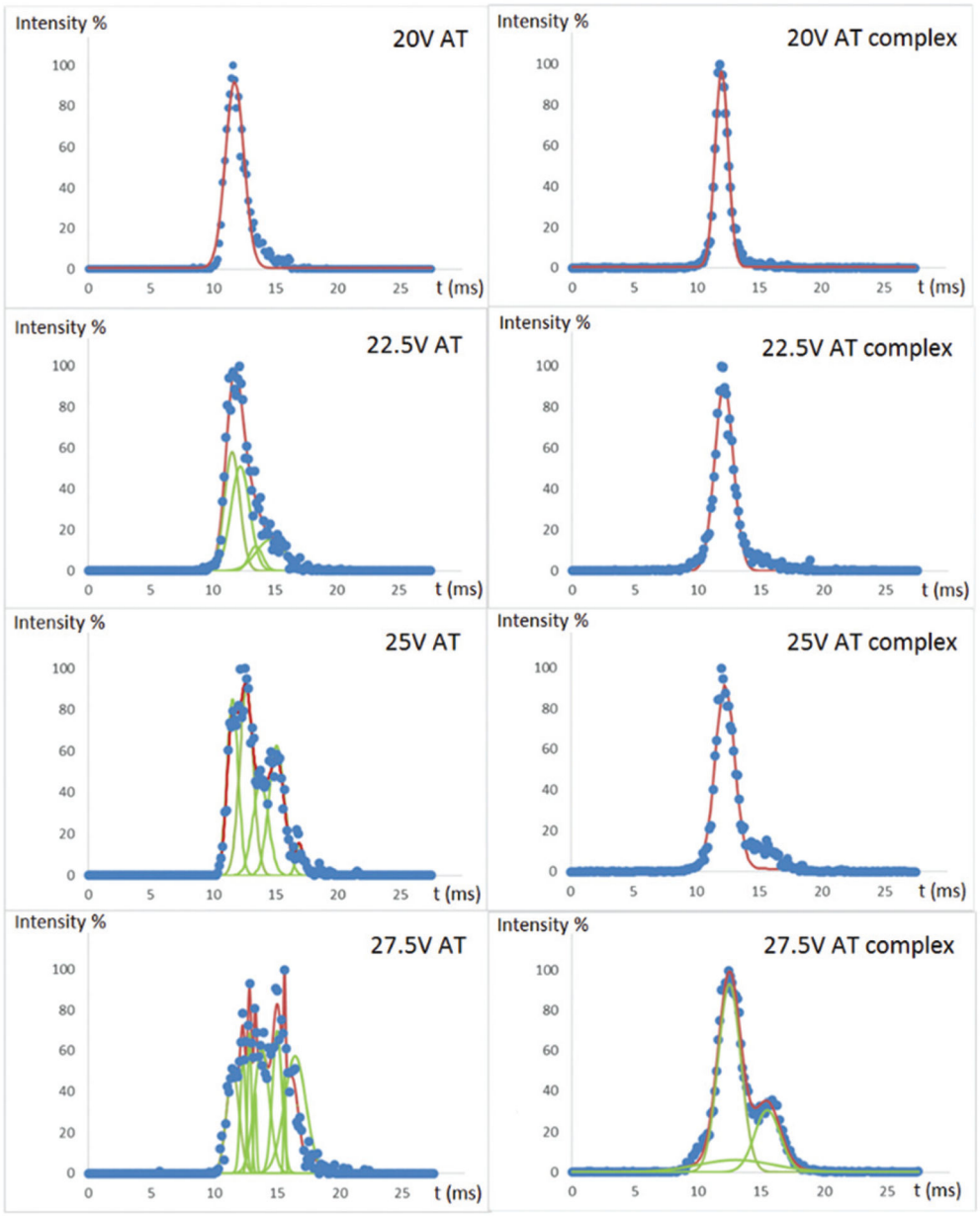

Fig. 7.

Experimental drift time distributions (ms) of +15 charge state of ATIII (left panels) and ATIII–Arixtra complex (right panels) as a function of trapping CE varying from 20 V to 27.5 V are shown in 2.5 V increments. The normalized experimental drift time distribution is shown by the blue dots. The fit of the data to a series of Gaussian distributions is shown in green, and the sum of the component Gaussians is shown in red.

Table 1

Calibrants

Calibrants and mass	Charge	CCS (He, Å^2)
Avidin	17	3640
64 kDa	18	3640
Concanavalin A	20	5550
102 kDa	21	5550
	22	5480
	23	5450
Cytochrome c	11	2303
12.4 kDa	12	2335
	13	2391
	14	2473
	15	2579
	16	2679
	17	2723
	18	2766
	19	2800
Myoglobin	15	3230
17.6 kDa	16	3313
	17	3384
	18	3489
	19	3570
	20	3682
	21	3792
	22	3815
Bovine serum albumin	15	4100
66.5 kDa	16	4060
	17	4040

Table 2

CCSs measured experimentally

Charge state	Free ATIII CCS (Å^2)	Arixtra-bound ATIII CCS (Å^2)	CCS increase (Å^2)	CCS increase %
14	3467.9 ± 14.5	3607.1 ± 16.6	123.5 ± 6.6	3.4
15	3439.8 ± 8.1	3573.1 ± 7.0	133.2 ± 2.3	3.7
16	3462.3 ± 17.6	3591.4 ± 15.9	133.0 ± 8.4	3.7

Table 3

CCSs calculated using MOBCAL

System	PA method (Å^2)	TM method (Å^2)
ATIII–Arixtra complex	3120.2 ± 3.2	4033.3 ± 14.5
ATIII	3010.1 ± 2.7	3900.5 ± 9.7
CCS increase%	3.7	3.4